Journal of Energy Storage 15 (2018) 359–367

Contents lists available at ScienceDirect

Journal of Energy Storage

journal homepage: www.elsevier.com/locate/est

Optimal pulse-modulated Lithium-ion battery charging: Algorithms and simulation

Huazhen Fang[a,*], Christopher Depcik[a], Vadim Lvovich[b]

[a] Department of Mechanical Engineering, University of Kansas, Lawrence, KS 66045, USA
[b] NASA John H. Glenn Research Center, Cleveland, OH 44135, USA

ARTICLE INFO

Article history:
Received 29 July 2017
Received in revised form 7 November 2017
Accepted 8 November 2017
Available online 7 February 2018

Keywords:
Pulse charging
Charging management
Battery management
Fast charging
Control theory

ABSTRACT

This paper focuses on the development of optimized pulse charging strategies for Lithium-ion (Li-ion) batteries. Aiming to improve the constant pulse charging in wide use today, we propose for the first time to modulate the current pulses during the charging process to reconcile health protection with charging pace. Toward this end, we use an equivalent circuit model and then formulate the problem of optimal pulse charging with an awareness of both battery health and charging speed. We then propose to resolve it using the linear control theory and obtain two charging methods, which regulate the magnitude and width, respectively, of the current pulses applied during the charging process. The proposed methods promise a two-fold benefit. First, the pulse-modulated charging will offer an effective means to defend the battery against the charging-induced harm to health without much compromise of the charging speed. Second, the methods have low computational cost, thus suitable for embedded battery management systems (BMSs) with constrained computing capabilities. This compares with the many charging techniques in the literature that require time-consuming constrained optimization. A detailed simulation study of the two proposed methods is offered to evaluate their effectiveness. The study endows pulse charging with a formalized design methodology unavailable before and impose a stronger health protection during its execution, which together can potentially translate into the momentum for its real-world application to Li-ion battery-powered systems including consumer electronics devices, electrical vehicles and solar photovoltaic arrays.

1. Introduction

Recent decades have seen a rapidly growing use of Lithium-ion (Li-ion) batteries, which have seen wide penetration in grid, renewable energy facilities and energy-efficient buildings. In these applications, battery management systems (BMSs) play the essential role of monitoring and regulating the operational status of the Li-ion batteries for improved performance, life, and safety [1,2]. A wealth of research of advanced BMS algorithms has thus come in response to this need. Prior, the focus was mainly on the state-of-charge (SoC) and state-of-health (SoH) estimation, aging status monitoring and thermal monitoring [2]. However, what has been less researched is the charging management, despite the consensus that improper charging protocol can cause fast capacity fade and a shortened life due to the fast build-up of internal stress and resistance, crystallization, and other negative effects [1,3–7].

*Literature review.*Charging by a constant current or a constant voltage is a popular industrial practice [8]. Yet, its relatively easy implementation comes at the expense of decrease in the battery cycle life. An improved approach is the constant-current/constant-voltage (CC/CV) charging [2,8]. Initially, a trickle charge (0.1 C or even smaller) is used for depleted cells, which produces a rise of the voltage. Then, a constant current (often between 0.2 C and 1 C) is applied. This stage ends when the voltage rises to a pre-specified level. It then switches to the constant voltage charging mode. The current diminishes in this mode, but the SoC continues to grow. In recent years, pulse charging has gained much interest among practitioners as an alternative beyond CC/CV. Its current profile is composed of pulses over time. Between two consecutive pulses is a short rest period, which allows the electrochemical reactions to stabilize by equalizing throughout the bulk of the electrode before the next charging pulse begins. This brief relaxation can bring multiple benefits to a Li-ion battery, including better charge acceptance, reduced gas reaction, inhibited dendrite growth, slowed capacity fade and faster charging rates [9–12].

* Corresponding author.
E-mail address: fang@ku.edu (H. Fang).

https://doi.org/10.1016/j.est.2017.11.007
2352-152X/

It is observed that these battery charging practices are inadequate for two reasons. First, they are empirical, with little knowledge available as to implementing them in the most optimal manner. For instance, determination of charge regimes for CC and CV modes, despite its importance for the performance of the CC/CV charging, has been mostly dependent on experience [13]. Second, they often operate as an open loop, simply taking energy from the power supply and failing to take into account the battery's history and current condition. These deficiencies limit the opportunity for maximum health protection during charging. To remedy them, a promising solution is to deploy the feedback control, which introduces a controller and closes the loop between the controller and battery. As such, the charging dynamics can be exploited, and the battery's charging profile optimized to enhance the charging process. In this area, optimal control in conjunction with electrochemical or equivalent circuit models has shown promise for optimizing charging protocols [14,3,15–17]. Model predictive control (MPC), which is also optimization-driven, represents another important class of methods with considerable interest because of its capability to handle health-relevant input, state, and temperature constraints. A few studies have been devoted to MPC-based charging in diverse settings [18–20]. In addition, adaptive control is investigated in [21] to craft an energy-efficient fast charging scheme, and sinusoidal charging studied in [22], which applies sinusoidal currents of the frequency minimizing the battery impedance. Optimal control design of charging/discharging of a battery during its operation is studied in [23] in order to maximize the work it can perform over a given duration while maintaining a desired final energy level.

Statement of contributions. The primary contribution of this work lies in the investigation of optimal pulse-modulated charging. In spite of recent advances as surveyed above, control-theory-enabled charging management is still at a nascent stage, requiring more effort in this direction. Among the various open problems, a prominent one is concerned with pulse charging. Although it has gained considerable popularity, there has been no systematic theoretical study about optimal design for pulse width and magnitude modulation to improve charging performance. To fill this gap, we leverage the linear control theory to develop optimal pulse charging solutions capable of balancing battery health protection and charging speed. Two methods will be obtained: the first one, named `PAM-C`, performs optimal pulse amplitude modulation (PAM) throughout the charging process, and the second, named `PWM-C`, optimally modulates the pulse width. In addition to the benefit of enhanced health protection, the proposed methods have a concise formulation and computational efficiency, suitable for real-time embedded BMS platforms. This work is the first one we are aware of that formalizes and optimizes the pulse charging design, with a potential for transforming its practical use in a wide range of battery systems. It will also provide further incentives for the advancement of battery charging technology.

Organization. The rest of the paper is organized as follows. Section 2 introduces an equivalent circuit model oriented toward charging dynamics. Based on this model, optimal pulse charging strategies will be developed and discussed subsequently in Section 3. To demonstrate effectiveness of the design, numerical results are then presented in Section 4. Finally, concluding remarks are gathered in Section 5.

2. Resistance-capacitance model for charging

Throughout the paper, we consider a second-order resistance-capacitance (RC) model proposed by SAFT Batteries, Inc. for high-power Li-ion batteries [24,25]. As shown in Fig. 1, it consists of two capacitors and three resistors. The resistor R_o represents the electrolytic resistance within a battery cell. The double RC circuits in parallel can simulate the migration of the electric charge during the charging (or discharging) processes. Specifically, the R_s–C_s circuit accounts for the electrode surface region, which is exposed to the electrode-electrolyte interface; the R_b–C_b circuit represents the bulk inner part of the electrode. Seeing a fast-speed transfer of the electric charge, the electrode surface is responsible for the high-frequency behavior during the charging processes and associated with the immediate amount of charge that the battery can absorb. However, it has a rather limited storage capacity. By contrast, the bulk electrode is where the majority of the electric charge is stored in chemical form. Since the diffusion of ions within the electrode proceeds at a relatively slower speed, the R_b–C_b circuit makes up the low-frequency part of the charging response. This implies that $R_b > R_s$ and $C_b \gg C_s$. While inductance can be present in a lithium-ion battery circuit, it manifests itself only at charging frequencies larger than 1 kHz [26], which indeed is far outside of the effecting frequency of the pulse charging mechanisms to be presented in this paper. This makes it unnecessary to include an inductive element in this model.

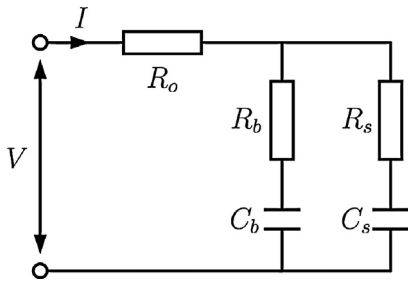

Fig. 1. RC-based equivalent circuit model for battery charging.

Let Q_b and Q_s be the charge stored by C_b and C_s, respectively, and define them as the system state x. That is, $x(t) = \left[Q_b^\top(t)\, Q_s^\top(t)\right]^\top$. The state-space representation of the model is then given by

$$\dot{x}(t) = Ax(t) + Bu(t),\ y(t) = Cx(t) + Du(t), \tag{1}$$

where $u(t)$ is the charging current, $y(t)$ the terminal voltage, and

$$A = \begin{bmatrix} -\dfrac{1}{C_b(R_b+R_s)} & \dfrac{1}{C_s(R_b+R_s)} \\ \dfrac{1}{C_b(R_b+R_s)} & -\dfrac{1}{C_s(R_b+R_s)} \end{bmatrix},\ B = \begin{bmatrix} \dfrac{R_s}{R_b+R_s} \\ \dfrac{R_b}{R_b+R_s} \end{bmatrix},$$

$$C = \begin{bmatrix} \dfrac{R_s}{C_b(R_b+R_s)} & \dfrac{R_b}{C_s(R_b+R_s)} \end{bmatrix},\ D = R_o + \frac{R_bR_s}{R_b+R_s}.$$

Note that $u(t) > 0$ for charging, $u(t) < 0$ for discharging, and $u(t) = 0$ for idling. Derivation of (1) is based on the Kirchhoff's circuit laws and capacitor equation, please see [24] for details. It can be easily verified that this system is controllable, indicating the feasibility of steering the battery's state $x(t)$ to any practically possible point.

The above RC model is linear and straightforward, but it can satisfy the needs in many applications. This is because Li-ion battery systems, e.g., those in electric vehicles, need to limit the minimum and maximum SoC during operation [27,28] for the purposes of safety, life, and a consistent power capability. Within this SoC window, the battery behavior can be approximated as linear. Furthermore, one can draw a linkage between this model and the well-known single particle model (SPM) [29] — the charge transport in the RC model is analogous to the diffusion of ions within a spherical particle representing an electrode. This plain observation can be further expanded to the approximate equivalence between the model in Eq. (1) and the SPM, which is proven in [17].

For health considerations, we need to constrain the difference between V_b and V_s throughout a charging process. The potential difference $\tilde{V} = V_s - V_b$, arising when the charging begins, is tied with health detriment. The larger it is, the more potential harm charging will bring. This conclusion is due to the resemblance that $\tilde{V}$ bears to the gradient of the concentration of ions within an electrode. According to [17], there is an approximate mathematical equivalence between the RC model and the SPM, and the potential difference $\tilde{V}$ approximates the Li-ion concentration gradient in the SPM. Created during charging, the concentration gradient drives the diffusion of ions. However, too large a gradient value will cause internal stress build-up, heating, solid-electrolyte interphase (SEI) formation, and other negative side effects [30–32]. An elaborative investigation is offered in [33] that studies how the gradient in Li-ion concentration affects the Li-ion insertion process and consequently, the internal stress and crack growth. Mechanical degradation in the electrode and capacity fade can happen or accelerate when the magnitude of the gradient is too large. Thus, the uneven ion concentration should be suppressed during charging. In addition, this restriction should be implemented more strictly as the SoC increases, when the battery becomes more vulnerable to the adverse effects caused by a large concentration difference [33].

It has been noticed that the pulse charging was indeed intended to mitigate the build-up of the concentration gradient [34,35] because the short rest period of a pulse cycle will allow for the ions to diffuse and distribute more evenly throughout the battery electrodes. In this work, we seek to maximize the potential of this "pulse-enhanced healthy charging" notion, through the design of optimal pulse modulation. Based on the above RC model, we will develop pulse-modulated charging methods, which can send energy into a battery in a health-aware manner but without significant compromise of the charging speed.

3. Optimal pulse charging

Despite the popularity of pulse charging, there have been scarce studies about how to regulate the pulse charging process to extract the full potential of this method. In this section, we will adopt a control-theoretic approach to bridge this divide and develop two methods, named `PAM-C` and `PWM-C`, which adjust the pulse amplitude and width, respectively, during the charging operation for the optimal performance.

Consider the current pulse signal $u(t)$ shown in Fig. 2. It has a period of T, an active duration of $w \in (0, T]$, and a magnitude of $M > 0$ during the active cycle; e.g.,

$$\begin{cases} u(kT+s) = M, & \text{for } s \in [0, w), \\ u(kT+s) = 0, & \text{for } s \in [w, T), \end{cases} \tag{2}$$

where k is a non-negative integer denoting the time index, and s an intermediate time variable. Modulation of the pulse refers to adjustment of the two variables w and M. Suppose that the pulse is applied to the model in Eq. (1) when $t = kT$. Then, according to [36], the state response during $[kT, (k+1)T)$ is given by

$$\begin{cases} x(kT+s) = e^{As}x(kT) + \int_0^s e^{A\tau}\mathrm{d}\tau BM, \text{for } s \in [0, w), \\ x(kT+s) = e^{A(s-w)}x(kT+w), \text{ for } s \in [w, T), \end{cases} \tag{3}$$

where τ is an intermediate integral variable. It is noted that Eq. (3) depicts a state evolution that consists of two stages. In the first stage, for $t \in [kT, kT+w)$, both elements of $x(t)$ will increase driven by the pulse current; whereas, the potential difference between C_b and C_s will grow accordingly, which can be expressed by

$$\tilde{V}(t) = V_s(t) - V_b(t) = Ex(t),$$

with $E = \left[-\frac{1}{C_b} \quad \frac{1}{C_s}\right]$. Under zero input in the second stage, the charge will migrate from C_s to C_b driven by $\tilde{V}(t)$, and meanwhile, $\tilde{V}(t)$ will be in gradual decline. From the electrochemical perspective, this mirrors the equalization of electrochemical reactions across the electrode, allowing for a catch-up with the transmittance of electric energy. The result will be mitigation of detrimental effects and build-up of the potential difference.

At time $t = kT$, the following cost function to minimize for optimal pulse charging is defined:

$$\begin{aligned} J(w, M, kT) &= \alpha\left(\int_{kT}^{(k+1)T} \tilde{V}(t)\mathrm{d}t\right)^2 + \frac{\beta}{w^2M^2} \\ &= \alpha\left(\int_{kT}^{(k+1)T} Ex(t)\mathrm{d}t\right)^2 + \frac{\beta}{w^2M^2}, \end{aligned} \tag{4}$$

where α and β are scalar weight coefficients with $\alpha, \beta > 0$. The first term of J, weighted by α, is based on the cumulative potential difference during $[kT, (k+1)T)$, which should be constrained for battery health. Thus, it can be referred to as the health cost. The second term, weighted by β, monotonically decreases with wM, the amount of charge delivered into the battery during this period. This implies that it is a cost associated with the "charging sluggishness" indeed. We can see that minimizing J will simultaneously penalize the health and sluggishness costs, which will finally result in a trade-off between health protection and charging speed. This is aligned with our design goal of enabling pulse charging with an awareness of both health degradation and charging speed.

The selection of α and β is important for the generation of the charging profile. According to the expression of J, one can find that the minimization will only rely on the ratio between α and β, i.e., α/β, rather than their individual quantities. Thus, we can fix one of them and adjust the other one in practical weight selection. During the adjustment, it should be kept in mind that the larger the ratio, the stronger the health protection, and the milder the current profile. This is because α and β symbolize the respective importance of health and charging rate. To see this, one can consider the extreme cases. If $\alpha/\beta = 0$, the maximum wM will be sought to minimize J. Thus, this scenario will see zero emphasis on health protection and the most aggressive charging behavior. If $\alpha/\beta \to \infty$, the minimization then will be only about the health cost, without any regard to the charging speed. The resultant minimizing solution will turn out to be zero current or no charging. In addition, we should also let $\alpha/\beta \gg 1$ in the practical implementation. This is intended to offset the difference of the α-weighted term and β-weighted term in the order of magnitude—$\left(\int_{kT}^{(k+1)T} \tilde{V}(t)\mathrm{d}t\right)^2$ typically coming at 10^{-3}–10^{-4} and $1/(wM)^2$ at 10^{-2}–10^{0}. If letting $\alpha/\beta \approx 1$ instead of $\alpha/\beta \gg 1$, the minimization of J will be more prone to penalizing the charging sluggishness, thus yielding too large a charging rate. A further discussion of how to select α and β is summarized in Remark 3.

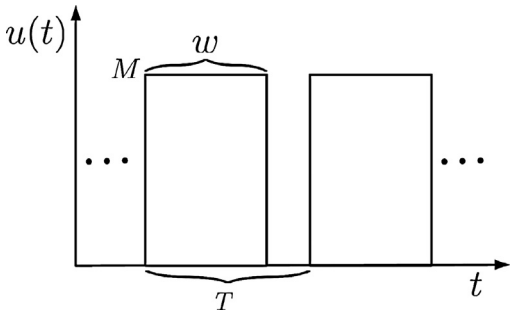

Fig. 2. Pulse signal for charging.

With the formulation of Eq. (4), the next question is to find w and M that can minimize J. To this end, we should express $J(w, M, kT)$ in explicit terms of w and M.

By the Cayley–Hamilton theorem [36], we can obtain

$$e^{As} = I + \frac{1 - e^{-(p+q)s}}{p+q}A,$$

where

$$p = \frac{1}{C_b(R_b + R_s)}, \quad q = \frac{1}{C_s(R_b + R_s)}.$$

It then follows from Eq. (3) that the state evolution during $[kT, kT + w)$ is governed by

$$x(kT+s) = \left[I + \frac{1 - e^{-(p+q)s}}{p+q}A\right]x(kT) + \left[sB + \frac{s}{p+q}AB + \frac{e^{-(p+q)s} - 1}{(p+q)^2}AB\right]M, \tag{5}$$

for $s \in [0, w)$. During $[kT + w, (k+1)T)$,

$$\begin{aligned} x(kT+s) &= e^{A(s-w)}x(kT+w) \\ &= e^{A(s-w)}\left(e^{Aw}x(kT) + \int_0^w e^{A\tau}\mathrm{d}\tau BM\right) \\ &= e^{As}\left(x(kT) + \int_0^w e^{A(\tau-w)}\mathrm{d}\tau BM\right) \\ &= e^{As}\left(x(kT) + \int_0^w e^{-A\tau}\mathrm{d}\tau BM\right) \\ &= \left(I + \frac{1 - e^{-(p+q)s}}{p+q}A\right)\left[x(kT) + \left(wI + \frac{w}{p+q}A - \frac{e^{(p+q)w} - 1}{(p+q)^2}A\right)BM\right]. \end{aligned} \tag{6}$$

Define the integration of the potential difference $Ex(t)$ over $[kT, (k+1)T)$ as

$$z(w, M, kT) = \int_{kT}^{(k+1)T} Ex(t)\mathrm{d}t. \tag{7}$$

It can be written as the summation of two components corresponding to the active and rest periods of a pulse cycle:

$$z(w, M, kT) = z_1(w, M, kT) + z_2(w, M, kT),$$

where

$$z_1(w, M, kT) = \int_{kT}^{kT+w} Ex(t)\mathrm{d}t,$$
$$z_2(w, M, kT) = \int_{kT+w}^{(k+1)T} Ex(t)\mathrm{d}t.$$

Using Eqs. (5) and (6), it is obtained that

$$\begin{aligned} z_1(\mathrm{w}, \mathrm{M}, \mathrm{kT}) &= \int_0^w Ex(kT+s)\mathrm{d}s \\ &= \left[wE + \frac{w}{p+q}EA + \frac{e^{-(p+q)w} - 1}{(p+q)^2}EA\right]x(kT) \\ &\quad + \left[\frac{w^2}{2}EB + \frac{w^2}{2(p+q)}EAB - \frac{w}{(p+q)^2}EAB - \frac{e^{-(p+q)w} - 1}{(p+q)^3}EAB\right]\mathrm{M}, \end{aligned} \tag{8}$$

$$\begin{aligned} z_2(w, M, kT) &= \int_w^T Ee^{A(s-w)}x(kT+w)\mathrm{d}s \\ &= \left[(T-w)E + \frac{(T-w)}{p+q}EA + \frac{e^{-(p+q)T} - e^{-(p+q)w}}{(p+q)^2}EA\right]x(kT) \\ &\quad + \left[(Tw - w^2)EB + \frac{Tw - w^2}{p+q}EAB - \frac{(e^{-(p+q)(T-w)} - 1)(e^{-(p+q)w} - 1)}{(p+q)^3}EAB\right]M. \end{aligned} \tag{9}$$

The relationship $A^2 = -(p+q)A$ is used in the above derivation of z_2. Inserting Eqs. (8)–(9) into Eq. (7) yields

$$z(w, M, kT) = \overline{A}x(kT) + h(w)M, \tag{10}$$

where

$$\overline{A} = TE + \frac{T}{p+q}EA + \frac{e^{-(p+q)T} - 1}{(p+q)^2}EA,$$

$$h(w) = \left(Tw - \frac{w^2}{2}\right)EB + \frac{Tw - \frac{w^2}{2}}{(p+q)}EAB - \frac{w}{(p+q)^2}EAB - \frac{e^{-(p+q)T} - e^{-(p+q)(T-w)}}{(p+q)^3}EAB.$$

Hence, $J(w, M, kT)$ in Eq. (4) can be rewritten as

$$J(w, M, kT) = \alpha[\overline{A}x(kT) + h(w)M]^2 + \frac{\beta}{w^2M^2}. \tag{11}$$

Even though the expression of $J(w, M, kT)$ is simplified as in Eq. (12), minimizing it with respect to w and M simultaneously is intractable. The first reason is the non-linearity involved, and what makes the matter worse is the non-convexity of J over the domain defined by w and M. However, J is convex with respect to w for $w \in [0, T]$ and also convex with respect to M for $M \in [0, \infty)$. The convexity results from the fact that, within the specified interval of w or M, the two terms of J are both convex. Hence, this implies the feasibility of fixing either w or M and conducting the optimization with respect to the other one, leading us to some viable solutions. The following two outcomes will be produced.

Pulse-amplitude-modulated charging (`PAM-C`). If we fix w, the pulse amplitude to apply at time kT can be determined readily. In this case, J will be convex with respect to M for $M \in (0, \infty)$. Thus, to find the minimizing M, we can let $\partial J/\partial M = 0$, which then gives the following quartic equation:

$$\alpha w^2 h^2(w)M^4 + \alpha\overline{A}x(kT)w^2h(w)M^3 - \beta = 0. \tag{12}$$

The properties of quartic equations have been well studied and documented in the literature, e.g., [37,38]. Based on the existing results, it can be determined that Eq. (13) has four roots, two real ones and two complex conjugate ones. Of the two real roots, one is positive and the other negative, and the positive root is the only meaningful solution for the considered problem since charging implies $M > 0$. The quartic equation can be analytically and efficiently solved using different methods [37,38], implying convenience for the execution of charging control.

It should be noted that the obtained M can be aggressive, especially in the beginning of the charging process, which may incur certain damaging effects. This motivates us to integrate bounded control with the practice of the pulse charging. That is, an upper bound, $M_{\max}$, for the charging current is pre-specified, and $M = M_{\max}$ enforced if the solution derived from solving (13) is larger than $M_{\max}$. Adding further protection against over aggressive charging, this effort will eliminate the risk imposed to the battery.

Pulse-width-modulated charging (`PWM-C`). Now, consider a fixed M and regulating the pulse width w. We notice that minimizing $J(w, M, kT)$ over w can be viewed as a nonlinear least squares problem, which can be addressed by the numerical Gauss-Newton algorithm. Define

$$r(w) = \begin{bmatrix} \sqrt{\alpha}[\overline{A}x(kT) + h(w)M] \\ \frac{\sqrt{\beta}}{wM} \end{bmatrix}.$$

The derivative of $r(w)$ with respect to w is

$$\nabla_w r(w) = \begin{bmatrix} \sqrt{\alpha}\nabla_w h(w)M \\ -\frac{\sqrt{\beta}}{w^2M} \end{bmatrix}$$

The Gauss–Newton proceeds by the following iteration procedure [39]

$$w^{(\ell+1)} = w^{(\ell)} - \rho\left[\nabla_w^\top r\left(w^{(\ell)}\right)\nabla_w r\left(w^{(\ell)}\right)\right]^{-1}\cdot\nabla_w^\top r\left(w^{(\ell)}\right)r\left(w^{(\ell)}\right), \quad (13)$$

where ℓ is the iteration number and $\rho \in (0,1)$ the step size. It can be initialized by $w^{(0)} = \delta$ for $\delta \in (0, T]$. On satisfaction of the stop condition, the iteration terminates, and the obtained $w^{(\ell)}$ will be assigned to $w(kT)$ as the width of the pulse to execute at time kT. Note that if the $w^{(\ell)}$ acquired in the final iteration is larger than T, then let $w(kT) = T$, which indicates that the battery status can tolerate full-duty-cycle pulse (continuous) charging in this stage. It is known that the Gauss-Newton algorithm can have a quadratic rate of convergence, so Eq. (13) can hopefully converge in several iterations. In addition, it is practically easy for one to choose an educated initial point for w since it lies in the interval $[0, T]$, which will speed up the convergence substantially.

The PAM–C and PWM–C methods offer two ways to perform pulse-modulated charging. A discussion of them is as follows.

Remark 1. Difference from the literature

This works differs from the methods in the literature in several aspects. First, this is the first work to our knowledge that is concerned with control-theory-based pulse charging design, which can help overcome empiricism in the practice of pulse charging. Second, the charging control design is based on an equivalent circuit model rather than electrochemical models often in the literature on charging control. Both models have their own advantages. But the mathematical conciseness of an ECM is key for computational efficiency. Form this viewpoint, the PAM–C and PWM–C methods are advantageous for deployment and use in resource-constrained computing platforms, such as real-time embedded BMSs. Finally, the primary health consideration in the proposed design is concerned with constraining potential difference, which is an approximation of the Li-ion concentration gradient. This is the first attempt in charging control design to our knowledge.

Remark 2. Computational efficiency

Eqs. (12) and (13) can be implemented efficiently from a computational point of view. This is advantageous to the deployment and use of the PAM–C and PWM–C methods especially in resource-constrained computing platforms, such as real-time embedded BMSs, in comparison to constrained-optimization-based charging techniques; e.g., [3,14–16].

Remark 3. Practical application of PAM–C and PWM–C

To transition the PAM–C and PWM–C algorithms to practice, one first needs to identify the model parameters in order to obtain an accurate model. Parameter identification of the considered RC model has been investigated in [40], in which the identifiability is analyzed and a real-time parameter estimation algorithm developed with proven convergence. In addition, real-time state estimation will be necessary. The design of the PAM–C and PWM–C methods is premised on state feedback, which assumes that the state vector $x(kT)$ is known for each k. However, $x(kT)$ as the internal state of the battery is not directly measurable. To address this issue, we can replace $x(kT)$ with its estimate $\hat{x}(kT)$ acquired from the input and output measurements. This can be accomplished by the celebrated Kalman filter on account of its optimality and relatively easy execution. The application of the Kalman filter to battery estimation has been investigated prior in the literature, e.g., [41–44]. Realization of the PAM–C and PWM–C algorithms will need the development of power electronics devices, especially a controllable current source, which will require continued research.

Remark 4. Choice of α and β

When the weight coefficients α and β take different values, the charging profiles will change accordingly, highlighting the importance of finding appropriate α of β for the implementation of PAM–C and PWM–C. A basic guideline is as follows:

- $\alpha \gg \beta$, because the α-weighted term in J is an order of magnitude smaller than the β-weighted term.
- One can fix one of α and β and adjust the other parameter, as a result of the minimization of J relying only on the ratio between α and β as is evident from the expression of J and Eqs. (12) and (13). A convenient means is to adjust α with $\beta = 1$.
- The ratio α/β should increase gradually through the charging process to constrain the charging rate more strictly when the SoC grows, because of a battery's susceptibility increasing with SoC to the charging current.
- A larger α/β implies a stronger health protection and a less aggressive charging profile.

Remark 5. Extension to other models

The methodology developed in this work can be extended to other battery models. As an example, an extension to the SPM can be achieved by reducing the PDE equations to the linear state-space representation, formulating an optimization problem, and then solving by finding the best pulse width and/or amplitude. It is worth pointing out that extensions can be made to accommodate temperature dynamics as a means to suppress the charging-induced heat build-up. Specifically for the considered model in Eq. (1), a thermal coupling can be performed as shown in [40]. We can then follow similar lines to accomplish the pulse-modulated charging design based on the modified model.

4. Illustrative examples

In this section, we present two numerical examples to demonstrate the application of the proposed PAM–C and PWM–C methods. The following simulation setting is used:

- We consider a Lithium-ion battery described by the RC model in Fig. 1 with known parameters: $C_b = 82$kF,$R_b = 1.1$ mΩ, $C_s = 4.074$ kF, $R_s = 0.4$ mΩ, and $R_o = 1.2$ mΩ [24].
- The battery has a nominal capacity of 8 Ah, with the operating voltage ranging from 3.50 V to 3.85 V.
- The SoC before charging is 30% at the voltage of 3.605 V, and the cut-off voltage is 3.85 V.
- For PAM–C, two sets of parameters are used for evaluation and comparison: (1) $\alpha = 2\cdot 20^{3\cdot \mathrm{SoC}+1}$ and $\beta = 1$, and (2) $\alpha = 2\cdot 20^{4\cdot \mathrm{SoC}+1}$ and $\beta = 1$. For PWM–C, two parameter sets are also selected: (1) $\alpha = 20^{3\cdot \mathrm{SoC}+1}$ and $\beta = 1$, and (2) $\alpha = 2\cdot 20^{3\cdot \mathrm{SoC}+1}$ and $\beta = 1$. Here, they are selected according to the guideline offered in Remark 3 and through an empirical adjustment. Note that the α increasing with the SoC is meant to enable a health cost commensurate with the charge transferred into the battery, which will ensure sufficient health protection under a large SoC.
- The period T of the pulses is 0.5 s. The active duration w is set to be 0.4 s for PAM–C and varies with the charging status for PWM–C.
- The pulse magnitude is dynamically regulated for PAM–C as governed by the algorithm, yet upper bounded by $M_{\max} = 8$ A, equivalent to 1 C, to avoid over aggressive charging; for PWM–C, it

is fixed at 8 A. Note that the magnitude is recommended to be no more than 1 C in practice.

Example 1: Evaluation of PAM-C and PWM-C. The PAM-C method is executed under the setting defined above and demonstrated in Fig. 3. The left column of Fig. 3 sums up the results for the first $\alpha-\beta$ set, and the right column for the second set. The figures in both columns show similar trends but different numerical values. Let us take a look at the left column first. As shown in Fig. 3a, pulses of 8 A are applied at the initial stage of charging. This is because the the battery can allow for a large charging current when at a low SoC level but PAM-C is subjected to the pre-set bound $M_{\max} = 8$ A. After about half an hour, the pulse magnitude will decrease as the SoC grows over time. Weaker current pulses can bring less harm to the internal health of the battery after it has stored a significant amount of electric energy. The potential difference $V_s - V_b$, quantifying the charging-induced effect on health, is illustrated in Fig. 3c. Without surprise, it is kept at a stable level during the initial stage, due to the fixed pulse magnitude. Then, a steadily declining trend is seen, and the voltage difference at the termination of charging is remarkably lower than that at the initial stage. A magnified view further reveals a rise-drop pattern that repeats itself — the potential difference rises during the active charging duration and drops during the rest period in each pulse cycle. This prevents the build-up of the potential difference and helps mitigate damaging effects. The trajectory of the SoC is given in Fig. 3e. The charging process lasts about 1 hr before it ends, with the SoC reaching 97.48%. It is seen that the growth rate of the SoC gradually reduces, which is caused by the diminishing pulse magnitude in Fig. 3a. Now, consider the PAM-C method applied with the second $\alpha-\beta$ set and the figures on the right column. It is seen from Fig. 3b that the charging

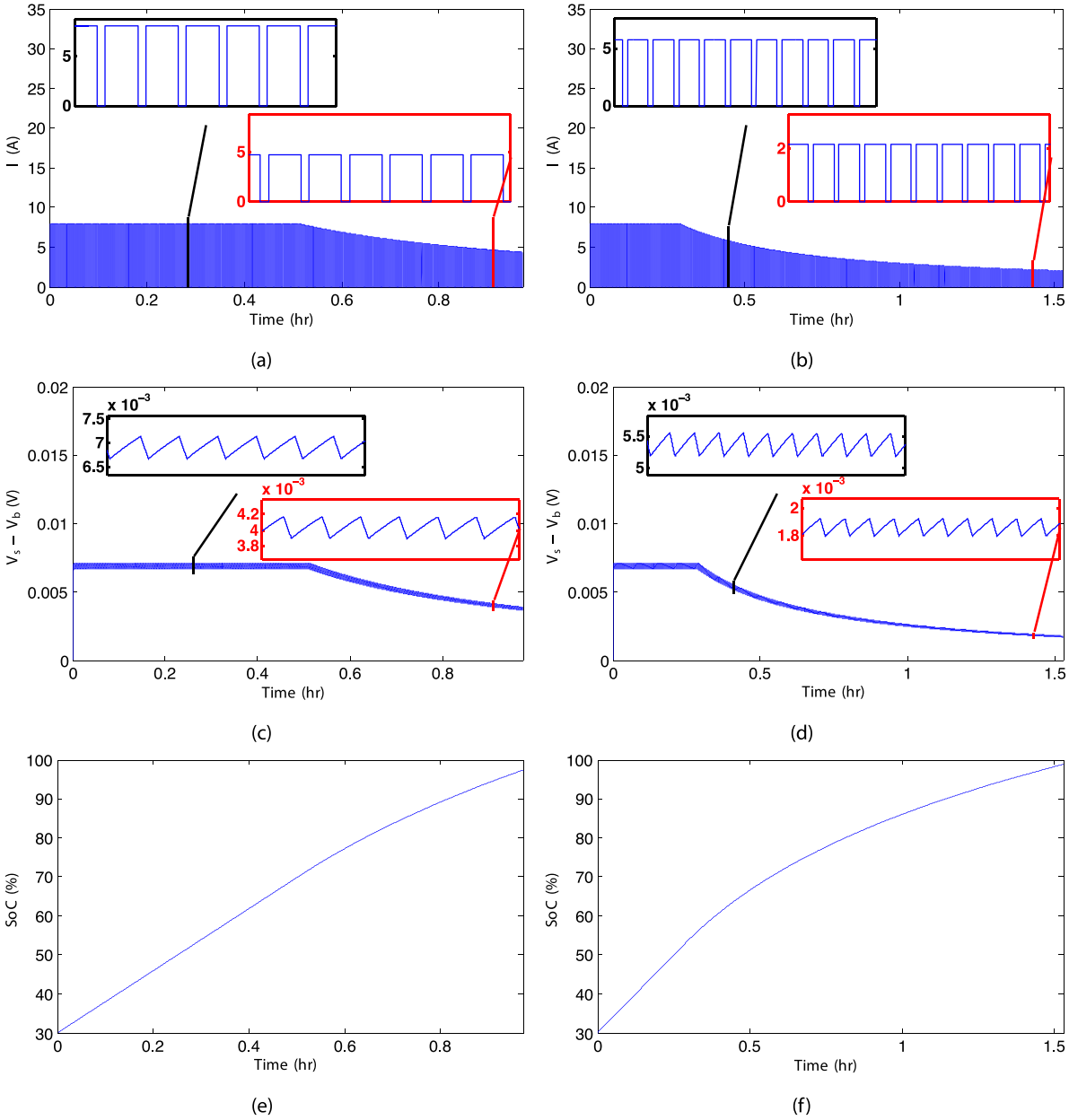

Fig. 3. Simulation of charging by PAM-C in Example 1. The left column is for the parameter set $\alpha = 2 \cdot 20^{3 \cdot \mathrm{SoC}+1}$ and $\beta = 1$, and the right column for $\alpha = 2 \cdot 20^{4 \cdot \mathrm{SoC}+1}$ and $\beta = 1$. (a-b) The PAM-C-generated charging current profile; (c-d) the resultant potential difference through time; (e-f) the resultant trajectory of the SoC through time.

aggressiveness in this case is suppressed more strictly, with the amplitude beginning to decline after only 0.3 h. This is caused by the appreciably larger ratio between α and β. The charging process as a result is increased to 1.5 h from 1 h in Fig. 3a. Meanwhile, the potential difference reduces to a lower level overall, as is shown in Fig. 3d, which implies potentially better health. Another benefit is that the SoC achieves 98.77% at the end of charging, about 1.31% higher than that shown in Fig. 3e. This shows that more energy can be put into a battery when the charging current is smaller.

The simulation of the PWM–C method using two parameter sets is given in Fig. 4. Let us begin with the left column for the first $\alpha-\beta$ set. From Fig. 4a, a constant current composed of full-duty-cycle pulses is applied in the first 0.2 h. That means the optimal w in this case is equal to T, which is possible because of the battery's ability to accommodate a high charging rate at a low-SoC level. This is followed by current pulses with decreasing widths, as illustrated in the magnified view. Resembling the downward trend of the magnitude in Fig. 3a, the decline of the pulse width is to reduce the risk of harm to the battery's health. The charging profile here shares certain similarity with the one used in [6], which experimentally verifies charging with a constant current first and then a series of pulses. The potential difference is shown in Fig. 4c. It remains almost constant at the beginning but decreases with the progress of charging, with the rise-drop pattern appearing in each pulse cycle. In Fig. 4e, the SoC rises and ends at 95.87% when the charging is terminated after 1 h upon the reach of the cut-off voltage. In the meantime, a decelerated SoC growth is observed, similar to Fig. 3e and meant to reduce the harm to the battery at high SoC. The right column presents figures for the second set of α and β. Fig. 3b illustrates that the increased ratio of α/β "abates" the charging process, with the active periods of the pulses reducing faster after the charging begins. According to

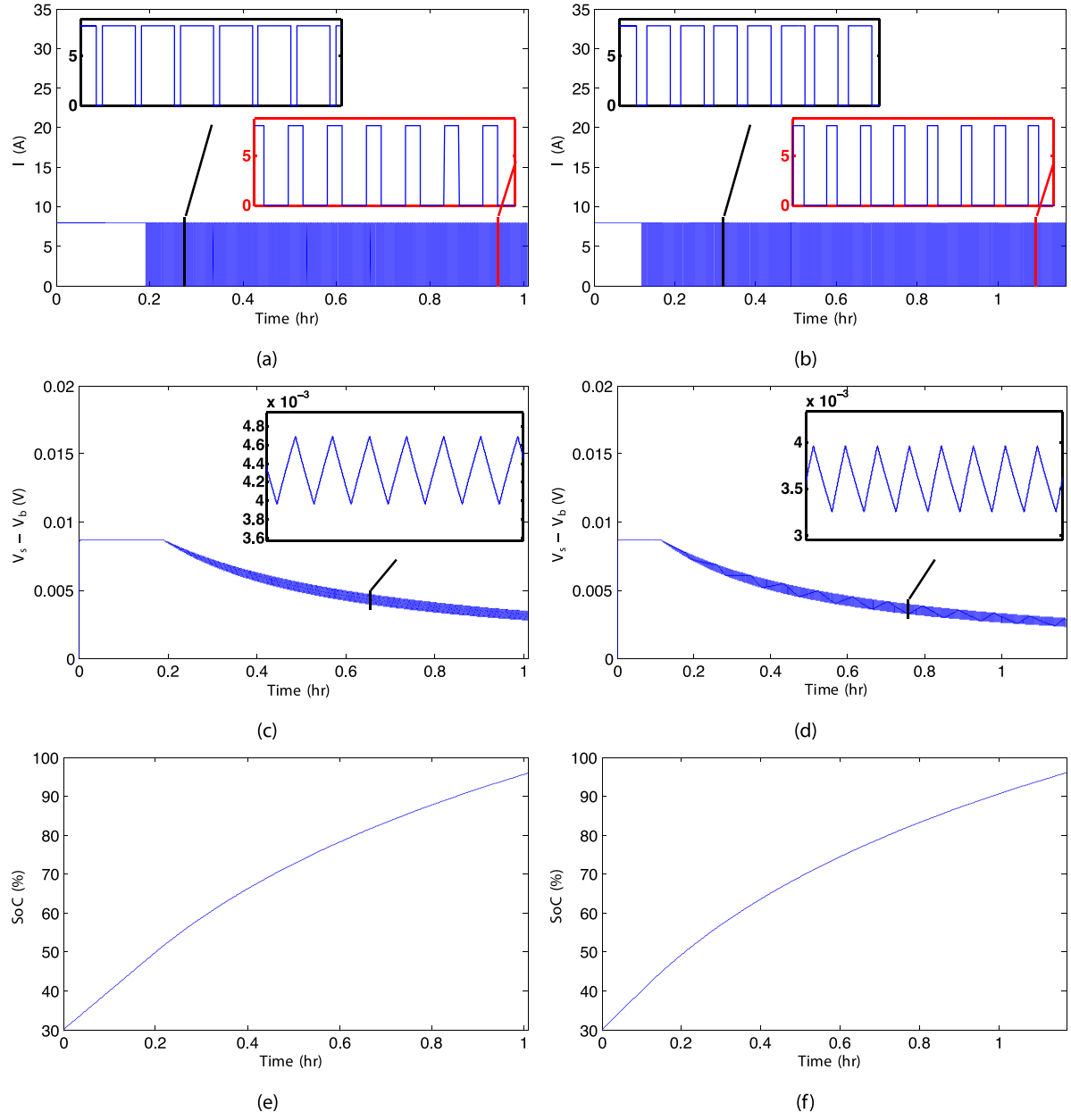

Fig. 4. Simulation of charging by PWM–C in Example 1. The left column is for the parameter set (1) $\alpha = 2 \cdot 20^{3\cdot SoC+1}$ and $\beta = 1$, and the right column for $\alpha = 2 \cdot 20^{3\cdot SoC+1}$ and $\beta = 1$. (a) and (b) The PWM–C-generated charging current profile; (c) and (d) the resultant potential difference through time; (e) and (f) the resultant trajectory of the SoC through time.

Fig. 4d and f, the potential difference level is more inhibited, and the final SoC increases slightly to 95.98% after 1.17 h of charging.

Example 2: Comparison with constant-pulse charging. This example assesses the PAM-C and PWM-C methods (each using its first parameter set in Example 1) through a comparison with the traditional constant-pulse charging (CPC). We assume the CPC method applies fixed periodic pulses. Their magnitude of 8 A, and the period is 0.5 s with an active duration of 0.4 s. In the simulation, it takes CPC 0.81 hrs to finish charging, which is modestly faster than both PAM-C and PWM-C. Fig. 5a compares the SoC-voltage profiles of PAM-C and CPC during the charging process. During the initial phase, the voltage yielded by PAM-C with respect to SoC is kept at a higher level than CPC, due to its large pulse magnitude. As

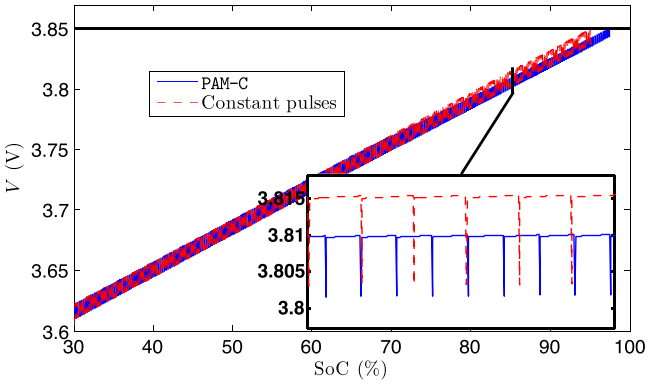

(a)

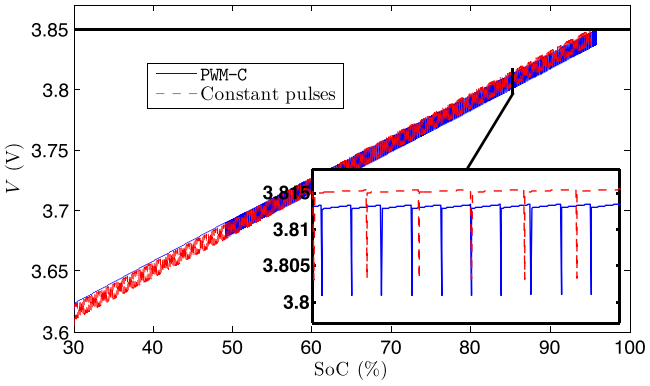

(b)

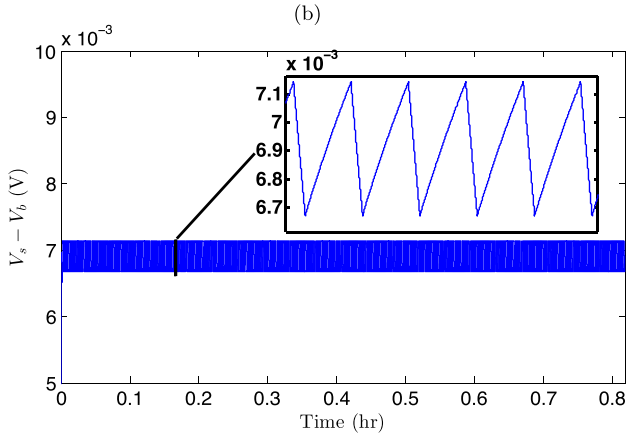

(c)

Fig. 5. Comparison of PAM-C and PWM-C with constant pulse charging (CPC) in Example 2: (a) the SoC-voltage profiles of PAM-C and CPC; (b) the SoC-voltage profiles of PWM-C and CPC; (c) the potential difference over time produced by CPC (compare with PAM-C in Fig. 3c and PWM-C in Fig. 4c).

the charging progresses, the PAM-C method reduces the magnitude gradually, and its potential difference ends up lower than that of CPC. This helps PAM-C put more charge into a battery, which is verified by the fact that the terminal SoC is 97.48% for PAM-C in contrast to 95.12% for CPC. Fig. 5b offers an examination of the PWM-C case. It is found that PWM-C can also improve the charge acceptance with the final SoC at 95.87%. Furthermore, Fig. 5c leads us to understand the major advantage of the PAM-C and PWM-C methods — better battery health protection. With CPC, the potential difference will be kept at higher than PAM-C and PWM-C for most of the charging process, especially in the latter part. This can cause internal damage when the SoC is large, placing the battery in potential jeopardy. Therefore, PAM-C and PWM-C outperform CPC in terms of health awareness and protection.

The above results are aligned with the anticipation that the pulse magnitude/width modulation can reduce the potential difference during charging to reduce health degradation. The simulation also results in several questions for further inquiry. Among them, the determination of the weight coefficients α and β needs more investigation as aforementioned. Another issue is the assessment and comparison of the PAM-C and PWM-C methods. As to which one of them is better, there is no clear-cut answer now because a few factors need to be taken into account, including charging speed, computational complexity, battery health, economic cost, and even user satisfaction. A plausible attempt to evaluate a charging approach will require a mix of theoretical and experimental examination, which will be part of our future quest.

5. Conclusion

This paper studies the problem of optimal pulse modulation for battery charging. We describe the charging dynamics using an RC model and consider the optimal regulation from a control-theoretic perspective. The design is built on minimizing a cost function that accounts for health cost and charging speed. It leads to two pulse charging methods, one based on pulse amplitude modulation and the other on pulse width modulation. We present a simulation-based examination of both methods that illustrates enhanced health protection and charge acceptance over prior methodologies. The results will not only benefit the real-world application of pulse charging, but also provide incentives for future research on control-theory-based charging and BMS design. Our future work will include the comprehensive assessment of the proposed methods and the extension of the design to other battery models and electrochemistries.

References

[1] H. Bergveld, W. Kruijt, P. Notten, Battery Management Systems: Design by Modeling, Springer, 2002.
[2] C.D. Rahn, C.-Y. Wang, Battery Systems Engineering, Wiley, 2013.
[3] B. Suthar, V. Ramadesigan, S. De, R.D. Braatz, V.R. Subramanian, Optimal charging profiles for mechanically constrained lithium-ion batteries, Phys. Chem. Chem. Phys. 16 (2013) 277–287.
[4] R. Spotnitz, Simulation of capacity fade in lithium-ion batteries, J. Power Sources 113 (2003) 72–80.
[5] M. Abdel Monem, K. Trad, N. Omar, O. Hegazy, B. Mantels, G. Mulder, P. Van den Bossche, J. Van Mierlo, Lithium-ion batteries: evaluation study of different charging methodologies based on aging process, Appl. Energy 152 (2015) 143–155.
[6] D.S. Hyun, H.J. Hwang, D.-U. Kim, S. Hwang, Y.-H. Yun, B.S. Oh, Development of an optimal charging algorithm of a Ni-MH battery for stationary fuel cell/battery hybrid system application, Int. J. Hydrogen Energy 38 (2013) 9008–9015.
[7] C. Wu, J. Chen, C. Xu, Z. Liu, Adaptive control strategy of a fuel cell/battery hybrid power system, Proceedings of American Control Conference (2016) 7492–7497.
[8] K. Young, C. Wang, L. Wang, K. Strunz, Electric vehicle battery technologies, in: R. Garcia-Valle, J.P. Lopes (Eds.), Electric Vehicle Integration into Modern Power Networks, Springer, 2012.

[9] L.T. Lam, H. Ozgun, O.V. Lim, J.A. Hamilton, L.H. Vu, D.G. Vella, D.A.J. Rand, Pulsed-current charging of lead/acid batteries – a possible means for overcoming premature capacity loss? J. Power Sources 53 (1995) 215–228.
[10] B.K. Purushothaman, U. Landau, Rapid charging of lithium-ion batteries using pulsed currents: a theoretical analysis, J. Electrochem. Soc. 153 (2006) A533–A542.
[11] A. Aryanfar, D. Brooks, B.V. Merinov, W.A. Goddard, A.J. Colussi, M.R. Hoffmann, Dynamics of lithium dendrite growth and inhibition: pulse charging experiments and Monte Carlo calculations, J. Phys. Chem. Lett. 5 (2014) 1721–1726.
[12] J. Li, E. Murphy, J. Winnick, P.A. Kohl, The effects of pulse charging on cycling characteristics of commercial lithium-ion batteries, J. Power Sources 102 (2001) 302–309.
[13] Y. Wong, W. Hurley, W. Wölfle, Charge regimes for valve-regulated lead-acid batteries: performance overview inclusive of temperature compensation, J. Power Sources 183 (2008) 783–791.
[14] R. Klein, N. Chaturvedi, J. Christensen, J. Ahmed, R. Findeisen, A. Kojic, Optimal charging strategies in lithium-ion battery, Proceedings of American Control Conference (2011) 382–387.
[15] J. Yan, G. Xu, H. Qian, Z. Song, Model predictive control-based fast charging for vehicular batteries, Energies (2011) 1178–1196.
[16] H. Perez, N. Shahmohammadhamedani, S. Moura, Enhanced performance of Li-ion batteries via modified reference governors and electrochemical models, IEEE/ASME Trans. Mechatron. (2015).
[17] H. Fang, Y. Wang, J. Chen, Health-aware and user-involved battery charging management for electric vehicles: linear quadratic strategies, IEEE Trans. Control Syst. Technol. 25 (2017) 911–923.
[18] M. Torchio, N.A. Wolff, D.M. Raimondo, L. Magni, U. Krewer, R.B. Gopaluni, J.A. Paulson, R.D. Braatz, Real-time model predictive control for the optimal charging of a lithium-ion battery, American Control Conference, (2015) , pp. 4536–4541.
[19] J. Liu, G. Li, H.K. Fathy, An extended differential flatness approach for the health-conscious nonlinear model predictive control of lithium-ion batteries, IEEE Trans. Control Syst. Technol. 25 (2017) 1882–1889.
[20] J. Liu, G. Li, H.K. Fathy, A computationally efficient approach for optimizing lithium-ion battery charging, ASME J. Dyn. Syst. Meas. Control 138 (2015) 021009-021009-8.
[21] R. Wai, S. Jhung, Design of energy-saving adaptive fast-charging control strategy for Li-Fe-PO_4 battery module, IET Power Electron. 5 (2012) 1684–1693.
[22] L.R. Chen, S.L. Wu, D.T. Shieh, T.R. Chen, Sinusoidal-ripple-current charging strategy and optimal charging frequency study for li-ion batteries, IEEE Trans. Ind. Electron. 60 (2013) 88–97.
[23] T. Wang, C.G. Cassandras, Optimal control of batteries with fully and partially available rechargeability, Automatica 48 (2012) 1658–1666.
[24] V.H. Johnson, A.A. Pesaran, T. Sack, Temperature-dependent battery models for high-power lithium-ion batteries, Proceedings of 17th Electric Vehicle Symposium (2000).
[25] V.H. Johnson, Battery performance models in ADVISOR, J. Power Sources 110 (2002) 321–329.
[26] F.C. Laman, M.W. Matsen, J.A.R. Stiles, Inductive impedance of a spirally wound Li/MoS2 cell, J. Electrochem. Soc. 133 (1986) 2441–2446.
[27] D. Knutsen, O. Willén, A study of electric vehicle charging patterns and range anxiety, Technical Report, Uppsala University, 2013.
[28] T. Markel, A. Simpson, Plug-in hybrid electric vehicle energy storage system design, Advanced Automotive Battery Conference (2006).
[29] S. Santhanagopalan, Q. Guo, P. Ramadass, R.E. White, Review of models for predicting the cycling performance of lithium ion batteries, J. Power Sources 156 (2006) 620–628.
[30] M.B. Pinsona, M.Z. Bazant, Theory of SEI formation in rechargeable batteries: capacity fade, accelerated aging and lifetime prediction, J. Electrochem. Soc. 160 (2013) A243–A250.
[31] W.H. Woodford IV, Electrochemical shock: Mechanical degradation of ion-intercalation materials, Massachusetts Institute of Technology, 2013 (Ph.D. thesis).
[32] T.M. Bandhauera, S. Garimellaa, T.F. Fullerb, A critical review of thermal issues in lithium-ion batteries, J. Electrochem. Soc. 158 (2011) R1–R25.
[33] M. Klinsmann, The Effects of Internal Stress and Lithium Transport on Fracture in Storage Materials in Lithium-Ion Batteries, Karlsruhe Institute of Technology, 2015 (Ph.D. thesis).
[34] R. Cope, Y. Podrazhansky, The art of battery charging, Proceedings of the Fourteenth Annual Battery Conference on Applications and Advances (1999) 233–235.
[35] R. Baroody, Evaluation of rapid electric battery charging techniques, University of Nevada, Las Vegas, 2009 (Master's thesis).
[36] C.-T. Chen, Linear System Theory and Design, 3rd ed., Oxford University Press, 2012.
[37] S. Neumark, Solution of Cubic and Quartic Equations, Pergamon Press, 1965.
[38] S.L. Shmakov, A universal method of solving quartic equations, Int. J. Pure Appl. Math. 71 (2011) 251–259.
[39] Å. Björck, Numerical Methods for Least Squares Problems, SIAM Press, 1996.
[40] M. Sitterly, L.Y. Wang, G. Yin, C. Wang, Enhanced identification of battery models for real-time battery management, IEEE Trans. Sustain. Energy 2 (2011) 300–308.
[41] X. Zhao, R.A. de Callafon, Modeling of battery dynamics and hysteresis for power delivery prediction and SOC estimation, Appl. Energy 180 (2016) 823–833.
[42] L. Zheng, L. Zhang, J. Zhu, G. Wang, J. Jiang, Co-estimation of state-of-charge, capacity and resistance for lithium-ion batteries based on a high-fidelity electrochemical model, Appl. Energy 180 (2016) 424–434.
[43] G.L. Plett, Extended Kalman filtering for battery management systems of lipb-based HEV battery packs: part 3. State and parameter estimation, J. Power Sources 134 (2004) 277–292.
[44] X. Lin, A.G. Stefanopoulou, Y. Li, R.D. Anderson, State of charge imbalance estimation for battery strings under reduced voltage sensing, IEEE Trans. Control Syst. Technol. 23 (2015) 1052–1062.